IL NUOVO CIMENTO Vol. ?, N. ? ?

SiPM: characterizations, modelling and VLSI front-end dedicated development

Davide Badoni(1)(2), Roberto Messi(1)(2), Vittorio Bidoli(2) Valerio Capuano(2) Marco Casolino(1)(2) Piergiorgio Picozza(1)(2) Alexander Popov(3)

(1) *INFN Structure of "Roma Tor Vergata"*
(2) *Physics Department, University of Roma "Tor Vergata"*
(3) *MEPHI, Moscow*

Summary. — In this work we describe the results of performance tests and measures of SiPM of several sizes ($1*1$, $3*3$, $5*5$) delivered from MEPHI. The SiPMs have been studied both in steady and pulsed stimuli. Aging and temperature behavior are also discussed. Another test have been performed in order to obtain an electrical model of the SiPM to be used in analog simulations. Finally, a design of a pilot chip with $0.35\mu m$ technology implementing a front-end for SiPM aimed to TOF applications with adjustable thresholds and very high dynamical range is described.

PACS 07.87.+v – Spaceborne and space research instrument.
PACS 95.55.Aq – Charge-coupled devices, image detectors, and IR detector arrays.
PACS 85.30.De – Semiconductor-device characterization, design, and modeling.
PACS 85.40.-e – Microelectronics: LSI, VLSI, ULSI; integrated circuit fabrication technology .

1. – Introduction

In this report we present the Silicon Photomultiplier (SiPM) characteristic, studied in both steady state and pulsed modes. We report also the study of a full custom Front End (FE) chip developed by INFN - Sez. Roma Tor Vergata in the framework of the Wizard collaboration. Furthermore we have studied the possibility to realize a TOF detector in space-based experiments taking into account power, mass and radiation resistance constraints. The SiPM is a good candidate detector for its fast response, good quantum efficiency, dimension and power consumption. We have studied three different diodes produced by MEPHI group ($1*1$, $3*3$ and $5*5$ mm^2) [1], [2]. The first and third type has been used to study the coupling SiPM-scintillator problems like efficiency, time response and different coupling topology. The $3*3$ mm^2 has good linearity response due to high pixel number and has therefore been used to determine the characteristic curves both in steady state current and in pulsed mode as function of temperature and integrated charges (aging). Our data set is obtained using two diodes $5*5$, six diodes $3*3$ and four $1*1$ SiPM. Furthermore we present the measures on the SiPM for modelling its electrical proprieties. This model has been used for the analog simulation of the analog VLSI front-end. We discuss this analog VLSI implementation of an prototype chip with eight channels aimed to TOF application with independent adjustable thresholds and wide dynamical range.

2. – Steady condition characteristics

We have studied the reduced gain $R.Gain$ as function of the working temperature and integrated charge. The usual definition of the gain is $G = \frac{(V_b - V_{BD})\, C_D}{q}$ (where V_b is the bias voltage and V_{BD} the breakdown voltage), contains the diode equivalent capacitance C_d and the initial charge q which is function to the number of fired pixel. The C_d parameter is measured by the technique described below. In order to measure the initial charge q we have to know the number of the incoming photons to the SiPM detector. Since we are interested to study the relative values of the Gain we have used the following definition: $R.\,Gain = \frac{I_{out}}{I_{in}}$ normally used for the APD [3] where I_{in} and I_{out} are respectively the current values for unitary gain ($V_b << V_{BD}$) and for gain equal to $R.\,Gain$ (V_b close V_{BD}). The I_{in} and I_{out} was also corrected for the dark current: $I_{in} = I_{inlight} - I_{indark}$ and $I_{out} = I_{outlight} - I_{outdark}$. This definition is valid only for gains lower than $300-500$, but is not valid for values above this limit where is not possible to define I_{in} correctly. In our case the I_{in} was defined by the condition $V_b << V_{bd}$ where all the characteristic curves (about 80) was linear and constant.

3. – Gain as function of the temperature

We have used a small cold finger liquid nitrogen cryostat at variable temperature. The SiPM detector was glued by silver-paint in the cold finger in order to have good thermal contact. The cold finger temperature was monitored by a platinum thermometer, while the SiPM temperature was monitored by silicon (Cryophysics DT470) thermometer glued very close to detector. All the apparatus was illustrated in fig.1.

Fig. 1. – Cold finger liquid nitrogen cryostat and SiPM-thermometer glued

In fig.2 are illustrated 14 dark current curves $I-V$ as function of the temperature ranging between $129\,K$ and $300\,K$. Two important points should be noticed: the first one is the decrease of V_{BD} in accordance to the temperature decrease; the second one is that below $230\,K$ the curves show a point of inflection, while above $230\,K$ show a quadratic behavior. Should be also noticed that the leakage current increases very fast for $T > 273\,K$. This is very important for future experimental application. Similar behavior is visible in fig.3 where the reduced gain is shown.

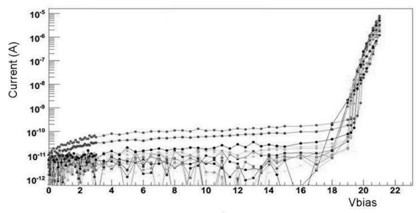

Fig. 2. – Dark current vs V_b as function of temperature

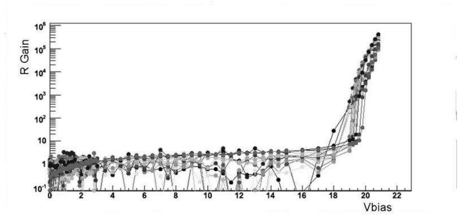

Fig. 3. – Dark R. Gain vs V_b as function of temperature

Comparing the last two plots is obvious that the reduced gain is an approximated definition. In fig.4 the reduced gain is show as function of the temperature (at fixed V_b). As shown, starting from 300 K, the gain increase as the temperature decrease: this is due both recombination process and free charges available. Is important to notice that is not useful to choose a working point below 260 K, obtained with a Peltier Cell or a CO_2 cooling system. Future investigation below 260 K should be done.

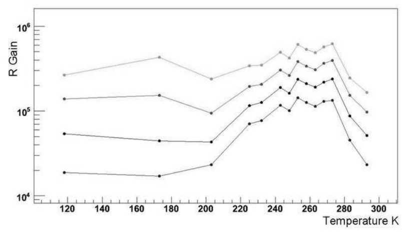

Fig. 4. – Last four highest R. Gain points for the curve in fig.3 as function of temperature

4. – Aging measurement

The aim of this measure should be investigate the behavior of the aging process as function of the integrate charge. We have used three diode $3 * 3$ in order to have a statistical significance. The experimental apparatus consist of a led in front the three SiPMs, we have choose a working point where the SiPM integrate $80\,mC/20\,min$, and the SiPM works in the linear region. The polarization of the SiPM is obtained by programmable Keithley 2410 power supply and the current was monitored by a Keithley 6514 picoamperometer connected to the computer system. For any point of integrated charge was measured two curves $I - V$ in dark and light condition in order to calculated the reduced gain (R gain). All this measure was done at constant temperature of $22\,C^{\circ}$. The total integrated charge was about $0.9\,C$. In fig.5 is shown the reduced gain as function of the V_b for different integrated charges. It is important to notice that the V_{BD} remain constant while the leakage increase, that means the intrinsic noise also increase.

In fig.6 is shown the reduced gain as function of the integrated charge (for three different values of V_b): the gain remain constant up to about $1\,C$. The first experimental point was made in different conditions.

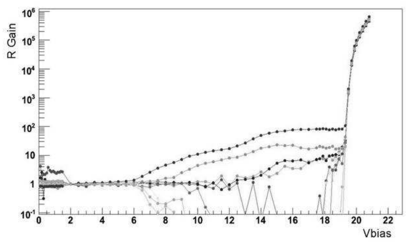

Fig. 5. – Behavior of the R Gain vs V_b curves as function of integrated charge from zero to 0.8 mC

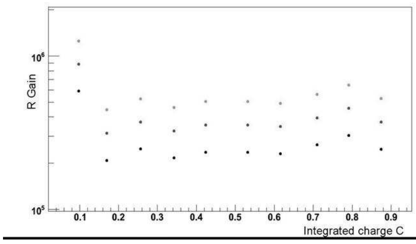

Fig. 6. – Last four highest R. Gain points for the curve in fig.5 as function of integrated charge

5. – Pulsed measure

In this case we have used the BTF at LNF, Frascati. We have used the three different available diodes in different topological coupling to BC408 scintillator (blue light emission around 400 nm). In fig.7 is shown the experimental apparatus where is visible the electromagnetic calorimeter which provides the number of electron in any bunch. Our apparatus is visible in the center of the system together with the trigger system and the beam pipe. The SiPM $1 * 1$ was coupled with the scintillator ($30 * 30\,mm^2$) through a wavelength shifter fiber (WLS Y11). These detectors were produced in the middle of 2004. The other SiPM (type $3 * 3$ and $5 * 5\,mm^2$) was glued close to the diametrically opposed corner of scintillator square slide ($75 * 75 * 5\,mm^3$). The linearity response of the detectors was fine for low signal, we present the results for all type of SiPM for a number max of 5 incident electrons on the scintillator (see fig.8). We have a good uniform response versus different area fired from electron bunch: in tab.**5** we show the sum of the analogical amplitude of two diametrically opposite SiPM function of different zone fired.

x / **y**	−30	0	+30
+12	119.1	123.6	120.4
0	120.6	124.6	120.3
−12			118.0

Table I. – *Amplitude of two diametrically opposite SiPM function of different zone fired*

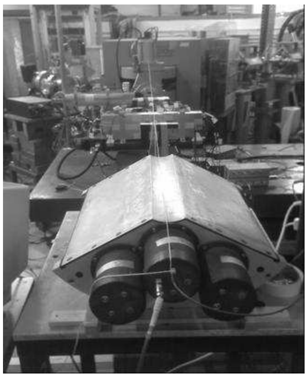

Fig. 7. – Esperimental apparatus at BTF electron facility at LNF

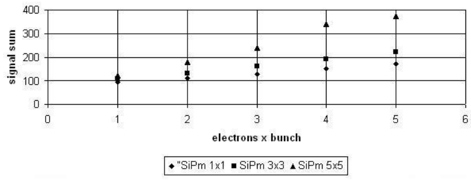

Fig. 8. – Dependence from delivery light detected

6. – SiPM model

Although SiPM have been available for many years, the analog electronics for optimization of some of its performance is still currently under study. A good model useful for a typical analog simulation in a VLSI project framework has been developed. This model takes in account the specific architecture of the SiPM consisting of several *pixels* connected in parallel all together. To make faster simulations using the SiPM models without degrade the reliability, it is a simplified model of the SiPM: in the architecture where some elements are omitted, and in the second order effects as after-pulsing or optical cross-talk that there are not modelled.

The first step for modelling is designing an equivalent circuit for the single pixel connected all together in parallel as shown in fig. 9. The $I_{dark_{pix}}$ takes in account the thermal current, it depends on temperature and bias voltage V_b and represent the time integral mean of the current. The $C_{d_{pix}}$ is the junction capacitance, it depends on V_b and on the deep of the depletion layer. The $R_{s_{pix}}$ is the ohmic resistor for the geiger mode current limitation. The $I_{ph_{pix}}$ is a current generator; it take in account the incoming photon(s): the time waveform is square and the time width has been fixed very short.

The constant recovery time of single pixel depend on C_pix and the series resistor composed by $R_{s_{pix}}$ plus the external loading resistor.

The choice of different amplitudes I allows to emulate the correspondent charge production: $Q(t) = I \cdot T$ which correspondent to different SiPM gain.

The parameters of the equivalent circuit have been derived from measures on the SiPM.

We assumed that parameters in all pixels are the same and that the array is equivalent to an circuit with the same architecture and parameters linearly scaled as shown in fig. 10. The event of n incoming photons which simultaneously arrives in different pixels can be obtain by multiply the generate current for n: $I_{ph}(n) = I_{ph} \cdot n$.

The equivalent circuit composed of the arrays of single pixels can be used in simulation with the advantage of make possible to reproduce a flow of incoming photons which arrives in a certain time; the disadvantage is that the simulation may be run slowly due to typical high number of pixels in array (i.e. 5625 in our used model).

The global equivalent circuit represented on the right side of the fig. 10 can be advantageously used in the simulation without substantially affecting the performance

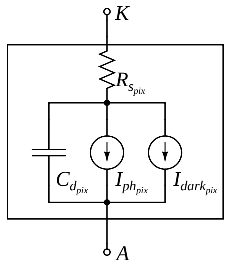

Fig. 9. – Equivalent circuit for the single pixel

of the simulation. The potential disadvantage is that is not possible consider a flow of n incoming photons arriving in a time comparable with the constant recovery time of the SiPM; the time width must be: or very short, in this case we use $I_{ph}(n)$ as mentioned before,; or the time between two incoming photons (or group) must be greater than the constant recovery time of the SiPM. We use the last choice for the development of front-end electronics since the project is oriented to a TOF application in space born experiment where the rate of events may be quite slow and the incoming photons relative to a single event can be consider simultaneous.

6˙1. *Procedure of the measures on SiPM for modelling.* – The parameter of the global model has been obtained through the experimental setup shown in fig.11.

All measures has been performed in dark light condition, so the dark current generator has not been considered. An low step voltage superimposed at the bias voltage has been applied to the SiPM. Through the oscilloscope the constant time has been measured; finally knowing the values of the series resistors, the value of the capacitance has been carried out. The measures has been repeated for several values of the V_b. The fig.12

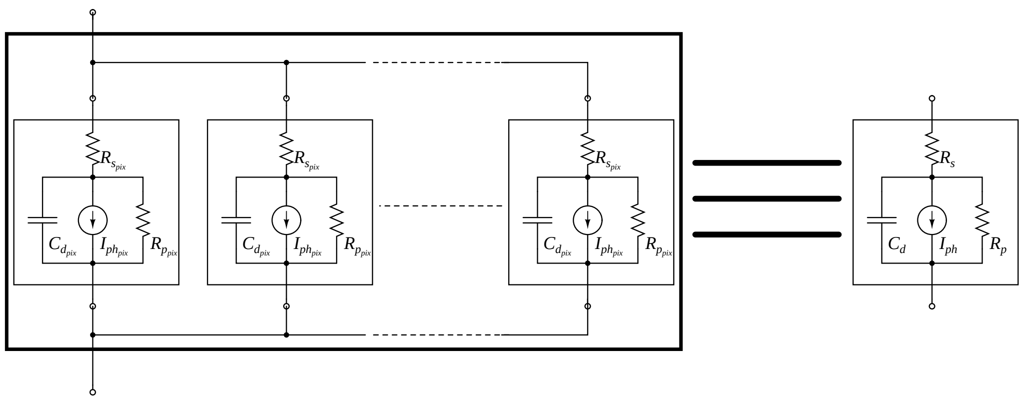

Fig. 10. – Equivalent circuit for the global model. With the approximation that parameters of all pixels are the same, the single pixel parameters (with *pix*) extension in the left side of the figure has a linear relationship with the parameters in the global representation in right side of figure

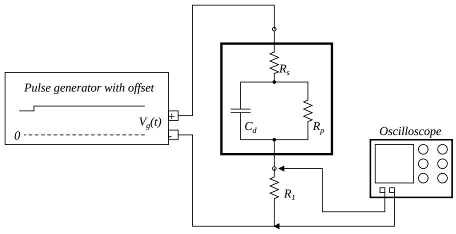

Fig. 11. – Experimental setup for the measures of the global parameter

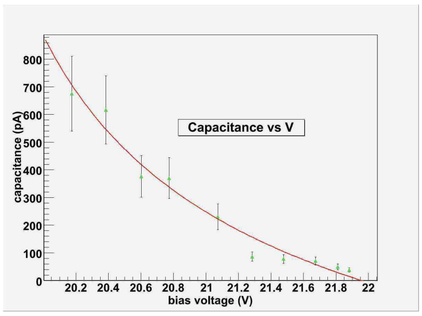

Fig. 12. – Relationship between the depletion capacitance and bias voltage V_b applied.

shown the relationship between capacitance and V_b. The measures fit well the relationship $C_d \approx \frac{1}{\sqrt{V_b}}$ as expected.

An important parameter of the SiPM is the linearity: the amplitude of signal vs the number n of the pixels stroked from simultaneous incoming photons. Named M the numbers of pixels of the array always is: maximum $n < M$. In the present work we have considered the data provide from MEPHI: for the $3 * 3$ SiPM with $M = 5625$ the range of linearity is nearly $1 - 1000$. We have fixed also the gain of SiPM at $400000\, e^-$.

7. – A analog VLSI front-end

This design has been developed with 0.35μ CMOS AMS technology. with four metals, two polysilicon layers a high resistivity layer.

It is intended for using in detecting time where the rate of the events are not high, in particular where the time between event is less then the time constant of the SiPM with its front-end. In such condition each event produces a current pulse where the height is proportional to the number of simultaneous incoming photons which is, finally, proportional at a Z^2 of the particle detected in the scintillator. Thus, we have developed an electronics with a large dynamical range and with a fast response of the front-end. This *double side* of this functionality permits to obtain a trigger from the event and a sort of *masking* for particles with a $Z < Z_{thr}$ where Z_{thr} is the minimum Z for producing a pulse. The threshold for Z is adjustable in a large dynamical range.

Once the loading impedance of the input preamplifier has been defined (which determines also the constant recovery time of SiPM), the peak value of the pulse generates from the SiPM for 1 pixel is also fixed.

With this scenario we choose the approach of *Current amplifier* for front-end since we would like a high dynamical range: namely $1 - -1000$ and a faster rise-time in input to the discriminator. These requirements are hard to satisfy with conventional voltage amplifiers. Also the recovery time of the complete system (SiPM with front-end) have to keep at the minimum: this implies a minimum dynamical series impedance at the SIPM. This requirement to match very well with the general low input impedance of a current amplifier.

The chip designed has to be considered as *pilot prototype chip* need for testing the *proposed analog circuits*.

We illustrate below the main significant circuit of the F.E..

In fig. 13 is shown the topological scheme of the preamplifier stage with its connections to the SiPM. The choice of fully-differential configuration assures a good immunity at the common-mode noise. Furthermore this configuration permits to introduce a current-feedback which improves twice the bandwidth (x 2) and the input impedance (x 1/2).

In fig.14 is shown the simplified schematic of one preamplifier. The current generators I_b and I_{bf} sets the quiescent point of the preamplifier. The input current coming in the p-mos in the branch on the left side is mirrored in the middle branch where a voltage-signal is available, also this signal drive the right branch where the feed-back current is generated. The *fully-balanced* [6] feature involves the coupling from branch: each branch is composed by only two mosfets (one is the current generator in the left and the right branches). This architecture is suitable for low-voltage applications and reduces the mismatch effects of the mosfets. [4], [5].

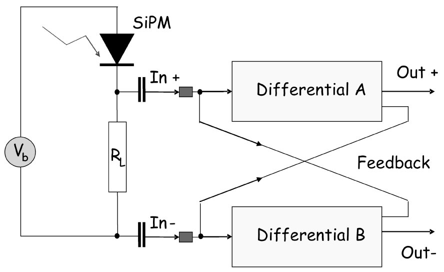

Fig. 13. – Fully differential current amplifier. Topological scheme

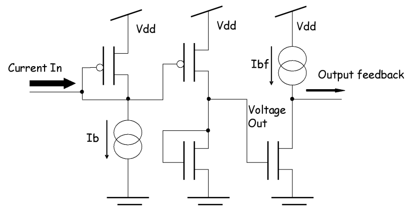

Fig. 14. – One side (A or B) of fully differential current amplifier: simplified schematic of *fully balanced* current amplifier

Other fundamental module is the discriminator: a fast current comparator [7]. As in the preamplifier, the current domain assures excellent performances in terms of speed and large dynamical range, which cannot be obtained with the correspondent voltage comparators. In fig. 15 is shown the simplified schematic of the current comparator. It is substantially a fast zero crossing. It works well both for low and high currents. An improved version of this comparator described in detail in [8] has been used. Since the discriminator is a single ended zero-crossing, we need to place a circuit between preamplifier and comparator to transform the differential output to a single-ended output. This solution does not degrade the features in respect at external common-mode noise immunity, and introduce only a very little sensitivity at the internal common-mode noise. The fig.16 show the circuit. It is composed of two stages: a simple differential pair and a current mirror.

7˙1. *General architecture of the chip.* – The general architecture of the prototype chip is shown in fig. 17. It consists in eight channels. Each channel include the *fully-differential current amplifier*, a *coupling circuit*, a *discriminator* (current-comparator), a *pulse-extender* modules and two analog buffers (one of this amplify ten times than the other one) in order to view the pulses on an oscilloscope. The *pulse extender* is a module which stretch out the time width of the output when it is too short: this happens in particular condition when the amplitude of SiPM signal is near to the threshold. The *bias generator* is the module which generates the reference currents for all internal current generators.

The current thresholds are independent for each channel.

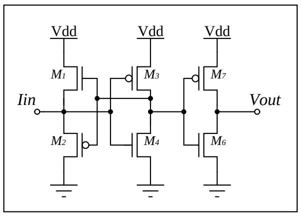

Fig. 15. – Fast current comparator

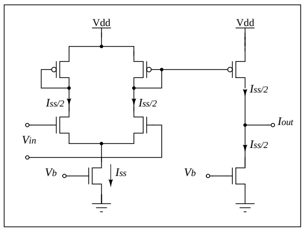

Fig. 16. – Coupling circuit. This circuit transform the output of preamplifier from differential to single-ended

8. – Results of simulations: performance

The above described circuit has been tested with typical, corners and Montecarlo analog simulations. The parameters under test are: 1)dynamical range of thresholds; 2)rise time in the input of comparator; 3)power consumption; 4) threshold offset; 5)estimation of the jitter; 6)linearity.

Concerning dynamical range of thresholds we obtain $160\mu A$ for a maximum of 1000 equivalent pixels, adjustable at step of 1 pixel and with a minimum value of 3 pixels. The rise rime is about $2\,ns$ and the power consumption is $16\,mW/channel$. The thresholds offset is shown in fig.18 as results of a *montecarlo simulation*, which provides an estimation on the offset current distribution on several channels on the same chip. Although the sigma is $9\mu A$ this is an acceptable value since a threshold is independently adjustable for each channel. The *corner simulation* shown a maximum of $-5 \div +15\mu A$ of current thresholds offset over all conditions simulated.

Concerning the jitter estimation we have considered the effect of intrinsic noise (coming from internal mosfet and resistor) as shown in fig.19 . A spectral analysis has been performed: the total equivalent noise has been calculated on the input comparator node. We have used this value inserting as a current constant perturbation. The resulting for

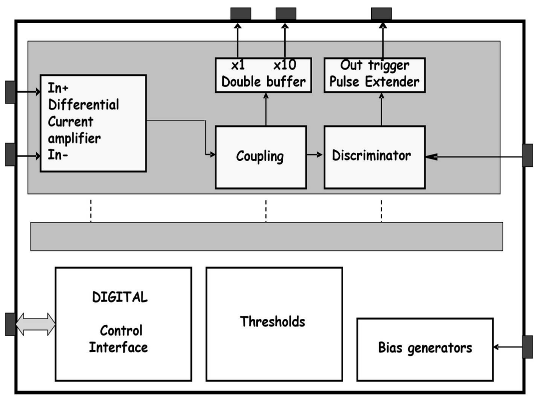

Fig. 17. – General architecture of the proposed chip

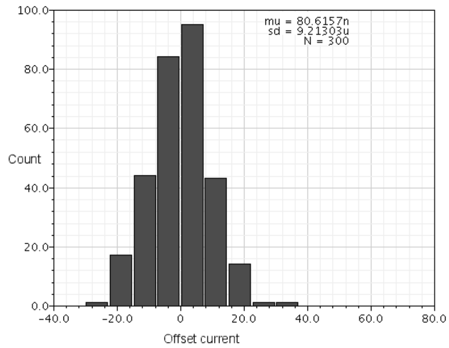

Fig. 18. – Montecarlo simulation: offset current distribution

jitter is J_{int} is: $20 < J_{int} < 50\,(ps)$.

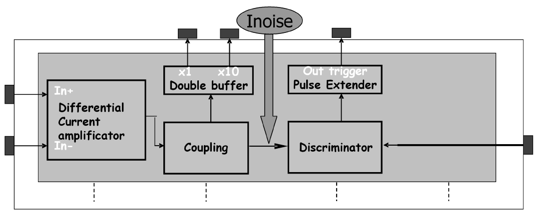

Fig. 19. – Intrinsic jitter estimation

The linearity, intended as maximum threshold vs amplitude of signal, is good and shown on fig.20.

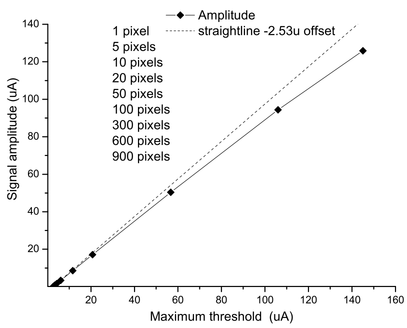

Fig. 20. – Linearity: the simulated point and the nearest straight-line with the same offset of $-2.53\,\mu A$

9. – Conclusion

We have studied the temperature characteristics and the beam test response of SiPM of various sized. We have investigate on the behavior of the aging process as function of the integrate charge: an important aspect resulting is that the gain remain constant up to about $1C$ of integrated charge. The behavior of characteristic of the diodes as function of the temperature ranging between $129\,K$ and $300\,K$ were investigated. We present the new behavior for a temperature range from $118K$ to $300K$. The leakage current increases very fast for $T > 273\,K$ and below of $230\,K$: the curves show an anomalous behavior. The test to the BTF in LNF at Frascati shown a good linearity and uniform response versus different area fired of different coupled SiPM-Scintillator type. Furthermore we have designed and simulated with success a chip with 8 channels of front-end for SiPM, aimed to TOF applications with independent adjustable thresholds and large dynamical range; the chip will be submitted on next September 2007 for production. The planned test on chip will be permits to adjust and consolidate the choice for the circuits.

REFERENCES

[1] Bondarenko G. and Dolgshein B., *Limited geiger-mode silicon photodiode with very high gain Nuclear Physics B*, **61B** (1998) 347

[2] Buzhan,P. and Dolgshein B., *Silicon photomultiplier and its possible applications Nucl. Instr. and Meth. A*, **A504** (2003) 48

[3] Karar A., Musienko Y. and Vanel J. Ch., *Characterization of avalanche photodiodes for calorimetry applications Nucl. Instr. and Meth. A*, **428** (1999) 413

[4] Sun B. and Yuan F., *New Low-Voltage Fully-Balanced Wide-Band Differential CMOS Current Amplifier*

[5] Sun B. and Yuan F., *A new differential CMOS current pre-amplifier for optical communication in Proc.of IEEE ISCAS'03*, **vol. 1** (May 2003) 341–344

[6] Sun B., Yuan F. and Opal A., *A New Differential CMOS Current-Mode Preamplier for GBps Data Communications Analog Integrated Circuits and Signal Processing*, **44** (2005) 191–201

[7] Traff H., *Novel Approach to High Speed CMOS Current Comparators Electronics Letters*, **vol. 28** (1992) 3 310–312

[8] Lin. H., Huang J.H. and Wong S.C., *A simple high-speed low current comparator IEEE International Symposium on Circuit and System*, (2000)